Midinfrared Extinction Spectra of Submicron Carbohydrate Particles Generated by a Pneumatic Atomizer†

Hideto Matsuoka,‡,§ Shinji Sekiguchi,‡ Kiyoshi Nishizawa,‡ and Toshinori Suzuki*,‡,||

Chemical Dynamics Laboratory, RIKEN, 2-1 Hirosawa, Wako, Saitama 351-0198, Japan, Institute of Multidisciplinary Research for Advanced Materials, Tohoku University, Katahira-2-1-1, Aobaku, Sendai 980-8577, Japan, and Department of Chemistry, Graduate School of Science, Kyoto University, Kyoto 606-8502, Japan

Received: January 5, 2009; Revised Manuscript Received: February 26, 2009

Carbohydrate aqueous solutions of trehalose, glucose, and fructose were sprayed by using a pneumatic atomizer, and their infrared extinction spectra were recorded for the region from 700 to 5000 cm^{-1}. Analysis based on Mie scattering theory indicated that sprayed droplets transformed into nonvolatile amorphous nanoparticles by solvent evaporation. Average diameters of these particles were estimated to be about 100 nm, which was further confirmed by differential mobility analysis. The results demonstrate that nanoparticles can be created by spray drying of aqueous solutions, and that the sizes, phases, and structures of these particles can be well characterized by infrared extinction spectroscopy.

Introduction

Almost half of the new chemical entities developed by the pharmaceutical industry are poorly water-soluble,[1] and their dissolution may be enhanced by transforming these chemicals into small particles, as it increases the surface areas.[2] Enhanced dissolution and absorption have already been proven for micrometer-sized drug particles,[3−5] and further improvement of solubility and bioavailability are expected for nanometer-sized particles. It has also been noted that nanoparticles may allow selective drug delivery into diseased tissues. Some reports indicate that particles smaller than 200 nm in diameter tend to accumulate in cancerous tissue considerably more than in normal tissues; this behavior is referred to as the enhanced permeability and retention effect.[6]

Conventionally, drug chemicals have been pulverized by crushing, grinding, and milling.[7] These procedures have rarely produced submicron particles. Although more recent techniques such as spray drying,[8] supercritical antisolvent technique,[9] and electrospray drying[10] produce submicron particles, these methods require heated gases, supercritical fluids, and high electric fields to enhance the evaporation of solvents. Electrospray also requires electroconductivity for the sample liquid. To create nanoparticles from a variety of solutions and enable their wider applications, a simpler and more robust liquid atomization method is necessary.

Carbohydrate−protein recognition plays an important role in a number of biological events, and some attempts have been made to utilize it to deliver drugs to specific tissues or cells.[11,12] Trehalose (Figure 1) has attracted attention from both fundamental and applied viewpoints for its bioprotective functions.[13,14] This interesting property is believed to arise from the characteristics described in its rich phase diagram[15] and possession of the highest glass-transition temperature of the amorphous phase among all disaccharides.[16−18] Trehalose is also a promising drug for polyglutamine diseases.[19] Previously, production of saccharide nanoparticles by electrospray of aqueous buffer solutions of glucose and fructose has been reported.[10]

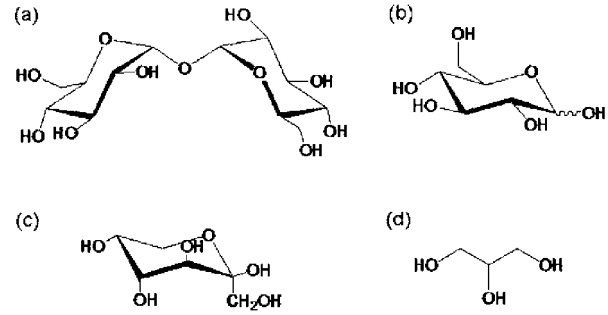

Figure 1. Molecular structure of (a) trehalose, (b) glucose, (c) fructose (pyranose form), and (d) glycerol.

In this work, we atomize aqueous solutions of saccharides using a pneumatic atomizer and characterize the sizes, phases, and structures of the nanoparticles generated by Fourier-transform infrared (FT-IR) extinction spectroscopy and differential mobility analysis (DMA). It is demonstrated that spontaneous solvent evaporation from the droplets efficiently creates amorphous particles ca. 100 nm in diameter.

Spectral Simulation

The extinction (absorption and scattering) of light by small particles depends on the size, shape, and number density of these particles.[20] Their spectrum is determined by a frequency-dependent complex refractive index $m(\nu)$. Here, m is defined as

$$m(\nu) = n(\nu) + ik(\nu) \quad (1)$$

where $n(\nu)$ and $k(\nu)$ represent the real and imaginary components of $m(\nu)$, respectively. The absorption and scattering of photons follows the Beer−Lambert law of extinction

† Part of the "George C. Schatz Festschrift".

* To whom correspondence should be addressed. E-mail: toshisuzuki@riken.jp.
‡ Chemical Dynamics Laboratory, RIKEN.
§ Tohoku University.
|| Kyoto University.

10.1021/jp9000835 CCC: $40.75
Published on Web 03/16/2009

$$-\ln \frac{I(\nu, d)}{I_0(\nu, d)} = (\alpha_{abs}(\nu, d) + \alpha_{sca}(\nu, d))L = E(\nu, d) \quad (2)$$

where I_0 is the intensity of the incident beam, I is the intensity after passing through the sample, d is the diameter of a particle, $\alpha_{abs}(\nu,d)$ and $\alpha_{sca}(\nu,d)$ are the absorption and scattering coefficients, respectively, and L is the length of the light path. Under our experimental conditions, the distribution of d is expressed by the following log-normal function

$$P(d) = \frac{D}{\sqrt{2\pi} d \ln \sigma_g} \exp\left[-\frac{1}{2}\left(\frac{\ln (d/d_g)}{\ln \sigma_g}\right)^2\right] \quad (3)$$

where d_g is the geometric mean diameter, σ_g (>1.0) is the geometric standard deviation, and D is the particle number density. The mode diameter d_M is defined by

$$\ln d_M = \ln d_g - \ln^2 \sigma_g \quad (4)$$

The absorption and scattering coefficients can be expressed as

$$\alpha_{ext}(\nu, d) = \alpha_{abs}(\nu, d) + \alpha_{sca}(\nu, d) = \frac{\pi d^2}{4} P(d)[Q_{abs}(\nu, d) + Q_{sca}(\nu, d)] \quad (5)$$

where $Q_{abs}(\nu,d)$ and $Q_{sca}(\nu,d)$ are the absorption and scattering efficiency factors, respectively. Mie theory provides the following efficiency factors for spherical particles:

$$Q_{sca} = \frac{2}{(\pi d\nu)^2} \sum_{N=1}^{\infty} (2N + 1)[|a_N|^2 + |b_N|^2] \quad (6)$$

$$Q_{ext} = \frac{2}{(\pi d\nu)^2} \mathrm{Re} \sum_{N=1}^{\infty} (2N + 1)[a_N + b_N] \quad (7)$$

$$Q_{abs} = Q_{ext} - Q_{sca} \quad (8)$$

where a_N and b_N are expressed in terms of Ricatti−Bessel functions. On the basis of Mie theory, we fitted $E(\nu,d)$ to reproduce experimental spectra. This implies that the particles were approximated as spherical.

We found that the nanoparticles were in the amorphous phase. Therefore, we measured the transmission spectrum of an amorphous layer prepared by a rapid air- drying method[21] and considered the spectrum to be the imaginary component $k(\nu)$ of nanoparticles in our spectral simulation using

$$k(\nu) = a \cdot \frac{\alpha_{abs}(\nu, d)}{4\pi\nu} \quad (9)$$

where a is an arbitrary scaling factor determined in the fitting procedure for our instrument and is independent of the concentration of the solutions. The real component $n(\nu)$ was calculated from $k(\nu)$ by using the Kramers−Kronig relation.[22,23] The frequency dependent cross sections of the extinctions weighted by the log-normal distribution function were calculated by modifying the BHMIE program of Bohren and Huffman.[20]

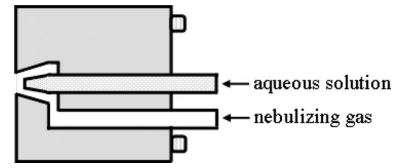

Figure 2. Schematic view of a homemade pneumatic atomizer.

The parameters (d_g, σ_g, and a) were optimized by least-squares fitting to the observed spectra.

Experimental Method

Saccharides (glycerol, trehalose, sucrose, and fructose) and distilled water were purchased from Wako Pure Chemical Industries, Ltd. and Kanto Chemical Co., respectively. Sample solutions were sprayed with a homemade pneumatic atomizer made of stainless steel. The atomizer is of an internal-mixing type, which discharges a liquid beam from a 20-μm orifice and a gas jet from an annular slit surrounding the liquid orifice (Figure 2). The liquid and gas flows collide inside the nozzle (internal mixing) and discharge together from the orifice 70 μm in diameter into the air. The liquid flow rate was controlled by an HPLC pump (Shimadzu LC-10AD). The flow rate and the pressure of the nebulizing gas (dry N_2) was 0.5 standard liter per minute (slm) at the stagnation pressure of 1 MPa. Infrared extinction spectra were recorded at a resolution of 0.6 cm^{-1} over a range from 700 to 5000 cm^{-1} with a Bruker VERTEX 80v vacuum FT-IR spectrometer equipped with a Globar light source, a KBr beam splitter, and an MCT detector. The optical compartment of the spectrometer was evacuated to eliminate IR absorption by atmospheric moisture. A multipass cell (Specac Ltd.) with an adjustable path length up to 10.6 m was employed. Since the original sample inlet was situated on the top of this commercial cell near the reflecting mirror, we added a new inlet on the side of the cell body that prevented the sprayed aerosols from contaminating the mirrors. The sample solutions were sprayed into the cell under atmospheric pressure from the atomizer nozzle attached to this new inlet. In this work, the path length was fixed to 10.6 m; however, since the atomized droplets travel perpendicularly to the propagation directions of infrared beams, the effective optical path length is expected to be much shorter than 10.6 m. Prior to spraying of the solutions, we have purged the cell with dry nitrogen gas to eliminate atmospheric water vapor and CO_2. The size distribution of the nanoparticles was estimated by Mie analysis and also by a commercial differential mobility analyzer with a Faraday cup detector (DMA, Wyckoff Co., Ltd.). We examined the droplet size distribution created by our pneumatic atomizer and that from a commercial atomizer (TOPAS, ATM 220) by DMA, and we found that they are similar to each other. However, the advantage of our atomizer is that it is operative at small flow rates, of the sample liquid and gas and atomization is possible in situ even in a low-pressure chamber.

Results and Discussion

DMA and FT-IR Measurements of Sprayed Trehalose Solutions. Figure 3 shows the FT-IR spectra observed by spraying aqueous solutions of trehalose with concentrations of (a) 0.5, (b) 1.0, (c) 5.0, and (d) 10.0 w/w %. A number of sharp lines appearing at around 1600 and 3900 cm^{-1} are the rotational structures associated with vibrational transitions of water vapor at room temperature. These gaseous water molecules were created in the cell by evaporation of the sprayed aqueous droplets and were unavoidable in our experiments. As the

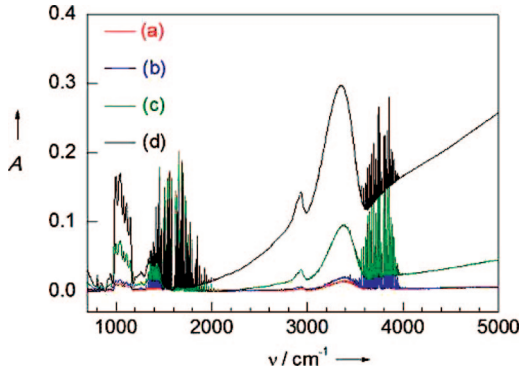

Figure 3. Midinfrared spectra of nanosized trehalose particles. The nanoparticles were produced by atomizing aqueous solutions of trehalose at a liquid flow rate of 50 μL/min and the nebulizing gas pressure of 1 MPa. The concentrations of trehalose aqueous solutions were (a) 0.5, (b) 1.0, (c) 5.0, and (d) 10.0 w/w %, which are shown by red, blue, green, and black lines, respectively.

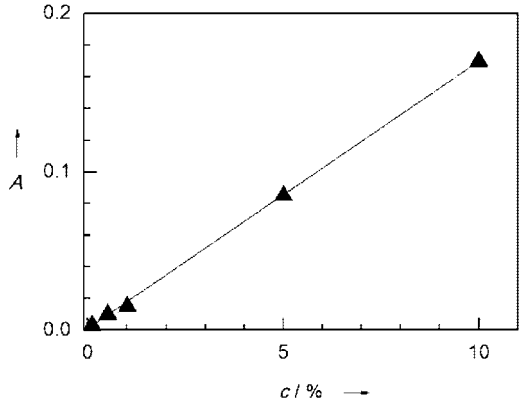

Figure 4. Concentration dependence of the absorbance of the OH stretching at 3400 cm^{-1} shown in Figure 3. Experimental values are indicated by triangles, and the solid line is a fitted linear function. The peak absorbance was obtained after light-scattering effects were subtracted from the spectra shown in Figure 3.

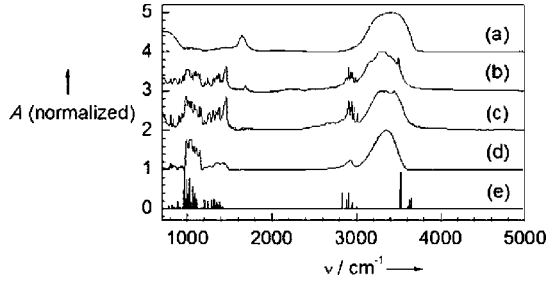

Figure 5. Observed midinfrared spectra of (a) a bulk aqueous solution of trehalose at 5 w/w %, (b) anhydrous trehalose, (c) the dihydrate, and (d) amorphous trehalose. The vibrational spectrum of trehalose calculated at the B3LYP/6-31G(d,p) level is shown as a line spectrum (e).

concentration of trehalose increases, broad absorption bands grow accordingly in the regions of 700−1600 and 2800−3600 cm^{-1}. As shown in Figure 4, the absorption intensity is proportional to the concentration of the sprayed aqueous solution. Therefore, these broad bands are attributed to trehalose. Figure 5 shows the FT-IR spectrum of (a) 5% aqueous solution, (b) crystalline anhydrous, and (c) crystalline trehalose dihydrate. Comparison of Figures 3 and 5 reveals the following differences. First, the spectrum of the aqueous solution (Figure 5a) is dominated by the absorption bands of liquid water, such as the strong bending band at 1640 cm^{-1}, while this is missing in Figure 3. This finding suggests that the sprayed samples do not contain much liquid-phase water. In other words, they have been dried. Second, the spectral features, such as the ones at around 2900 cm^{-1} of trehalose in Figure 3, are unstructured, while the spectra of crystalline samples shown in parts b and c of Figure 5 exhibit sharp features. Therefore, the sprayed samples are not crystals either. Thus, we conclude that the sprayed samples become amorphous solids. We have also carried out measurements by introducing a sample gas into the cell after flowing through a diffusion dryer (TSI 3062), and we found essentially the same spectra except for the reduced absorption intensity of water vapor.

In Figure 5b, the sharp stretching band observed at 3500 cm^{-1} is due to water molecules in the crystal, while the sharp peak at 1685 cm^{-1} is due to H−O−H bending. The H−O−H bending band of the crystal water was barely visible in the spectrum of the sprayed sample at 10.0 w/w % and unrecognizable in more diluted samples. This result suggests that residual water molecules do exist in the amorphous trehalose, however, at most at a similar ratio to that in the crystalline dihydrate. Figure 5d is the spectrum of bulk amorphous trehalose measured in the present work, which agrees very well with Figure 3.

In Figure 5e the vibrational spectrum of trehalose predicted by quantum chemical calculations is shown. Geometry optimization and vibrational analysis of trehalose were performed by using density functional theory at the B3LYP/6-31G(d,p) level with the GAUSSIAN 03 package. The initial geometry was taken from the crystal structure of trehalose anhydrous.[24] The vibrational frequencies were calculated with the harmonic approximation and scaled with a factor 0.9613 as recommended for B3LYP/6-31G(d) calculations.[25] The O−H stretching bands were predicted in the 3000 − 3800 cm^{-1} region. The C−H stretching bands were calculated to be in the frequency range from 2800 to 3000 cm^{-1}, being well separated from the H−C−H, C−C−H, and C−O−H bending bands between 1200 and 1450 cm^{-1}. The bridge C−O−C stretching modes were predicted between 900 and 1200 cm^{-1}. Comparing the infrared spectra of crystalline and amorphous trehalose, the former clearly exhibits much sharper features, which are attributed to the higher degree of homogeneity in the crystal. It is interesting that even C−H bands that are not involved in hydrogen bonding become diffuse in the amorphous form. The similarity between the fingerprint region in spectra of amorphous trehalose and of solutions suggests the resemblance in the intramolecular structures in these phases.

Another feature apparent in the spectra is the baseline rising toward higher wavenumbers. This is a consequence of light scattering, which means that the amorphous particles are larger than tens of nanometers in diameter. We employed Mie theory to interpret the FT-IR extinction spectra of the sprayed trehalose solution including infrared absorption and scattering components. In our analysis, the $E(\nu,d)$ in eq 2 was fitted to the experimental spectra by adjusting the log-normal distribution parameters d_g and σ_g. A single log-normal distribution was assumed. This fitting provided the best-fit parameter sets; however, it is important to pay attention to other likely solution sets. Figure 6a displays the sum of the squares of the residuals in the least-squares fitting of the FTIR spectrum of 1.0 w/w % trehalose aqueous solution. In the black-colored region, by assuming a log-normal distribution with corresponding d_g and σ_g, the calculated spectrum reproduced the experimental spectrum reasonably well. When the parameter sets in the black-colored region were examined further, the best-fit parameter to the experimental spectrum was identified, as indicated by the arrow in Figure 6b. The simulated spectra thus obtained are

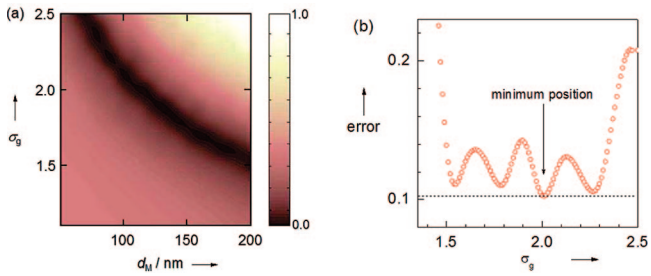

Figure 6. (a) A contour plot of the sum of the squares of the residuals corresponding to the deviation between the observed and calculated spectra of the aqueous solution of 1.0 w/w % trehalose. (b) The plot of the residuals in the black band region of part a vs. the geometric standard deviation σ_g.

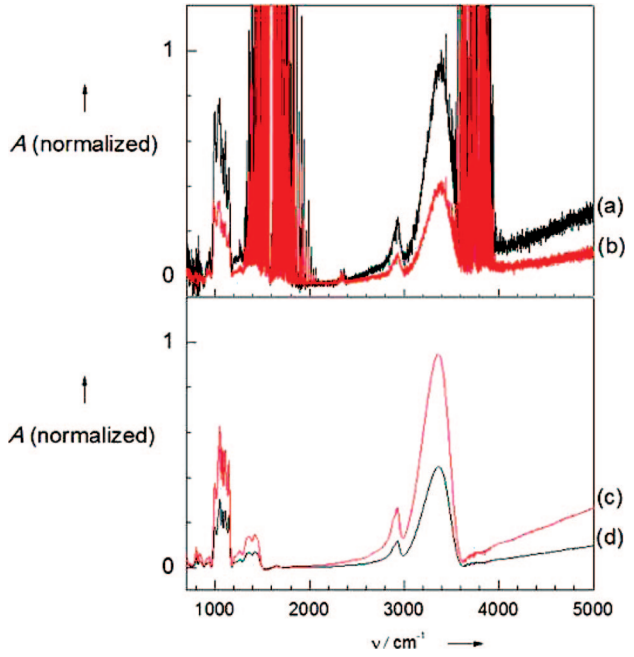

Figure 7. (a, b) Observed and (c, d) calculated midinfrared spectra of nanosized trehalose particles. The nanoparticles were produced by atomizing aqueous solutions of trehalose at a liquid flow rate of 50 μL/min and a nebulizing gas pressure of 1 MPa. The concentrations of aqueous solutions of trehalose were 0.5 w/w % in parts a and c and 1.0 w/w % in parts b and d.

shown in parts c and d in Figure 7 in comparison with the observed spectra, Figure 7a,b. The log-normal size distributions used in the simulations are shown in parts c and d of Figure 8.

The drawback of the size distribution deduced by Mie analysis of IR extinction spectra is that the uniqueness of the best-fit parameter is not completely ensured. To solve this problem, we have examined the size distribution independently by DMA. The size distributions of particles generated from aqueous solutions of trehalose at (a) 0.5 and (b) 1.0 w/w % determined by DMA are shown in parts a and b of Figure 8. The solutions were sprayed under atmospheric pressure. The average diameter of the particles was ~100 nm, and the distribution was almost log-normal. The DMA results are in good agreement with the distribution determined by Mie analysis of FTIR extinction spectra. It is interesting to examine whether the IR absorption spectrum of amorphous particles varies with their size. We extracted pure absorption spectra of nanoparticles by subtracting the scattering components from the observed extinction spectra. We found that the absorption spectrum of the particles is the same as that of bulk amorphous. This is understandable since the particle size is as large as 100 nm.

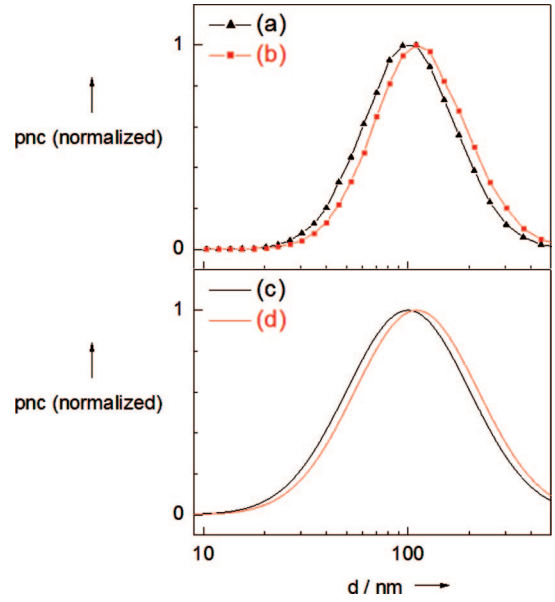

Figure 8. Particle size dependence of particle number concentration (pnc) of trehalose nanoparticles determined by DMA measurements (a, b) and Mie calculations (c, d). The concentrations of aqueous solutions of trehalose were 0.5 w/w % in parts a and c, and 1.0 w/w % in parts b and d.

Primary Droplet Sizes. The formation process of nanoparticles may be complex. Primary droplets presumably undergo breakup and coalescence upstream in the supersonic gas flow of dry nitrogen, and then these liquid droplets rapidly dry out. If we assume droplets no longer break up or coalesce during the drying process, the liquid droplet diameters prior to drying may be estimated from the diameters of the observed solid particles. Imamura et al. reported that the density of an amorphous matrix of trehalose is about 1.5 g/cm^3.[26] Assuming that the particles of the sprayed trehalose have the same density, the 100-nm particle is estimated to be an aggregate of about 1.4 million molecules of trehalose. The mean diameters of the amorphous solid particles were 100 and 110 nm as a result of spraying 0.5 and 1.0 w/w % trehalose in water, respectively. From these values, the liquid droplet diameters prior to drying are estimated to be 670 and 590 nm. This suggests that the liquid droplet diameters prior to drying are rather similar for different sample concentrations.

For comparison, we also atomized an aqueous solution of glycerol with the same atomizer. Glycerol (Figure 1d) is widely used in pharmaceutical formulations. Although glycerol is a liquid at room temperature, its vapor pressure is 1000 times smaller than that of water. The observed FT-IR spectra were reproduced reasonably well by Mie theory (not shown here), where the spectrum observed for the bulk solution of pure glycerol was used as the imaginary part of the refractive index. After spraying an aqueous solution of glycerol at 0.5 v/v %, the average particle diameter was estimated to be 100 nm by Mie analysis. The analysis has shown that only water molecules have evaporated from the droplets, producing nanosized droplets of pure (or highly concentrated) glycerol solution. The density for the bulk of liquid pure glycerol is about 1.26 g/cm.^{3} Assuming that all the particles of the sprayed glycerol have the same density, the particle 100 nm in diameter is composed of 4.3 million molecules of glycerol. This estimation indicates that the 100 nm particle was produced by spontaneous solvent evaporation from the droplet 600 nm in diameter when the aqueous solution of glycerol 0.5 v/v % was sprayed. This agrees

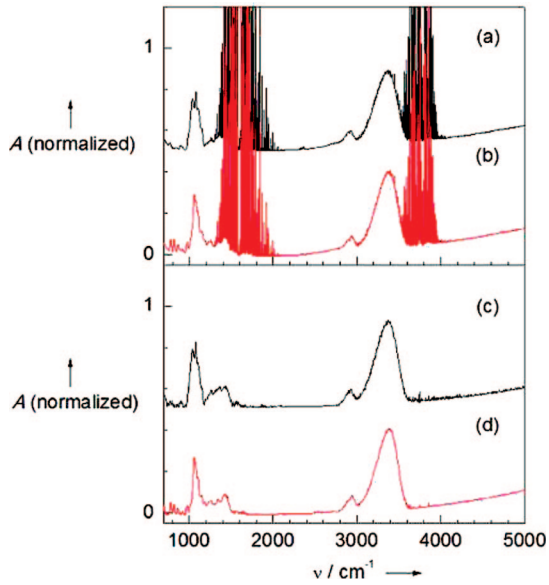

Figure 9. Experimental midinfrared extinction spectra of (a) glucose and (b) fructose particles produced by spraying 1.0 w/w % aqueous solutions. The Mie simulations of parts a and b are shown in parts c and d, respectively. The mode diameters and geometric standard deviations used in the calculations are (c) 110 nm and 1.2 and (d) 100 nm and 1.5.

with the previous estimation of the primary droplet size for a trehalose solution.

DMA and FT-IR Measurements of Sprayed Glucose and Fructose Solutions. Solid lines in parts a and b of Figure 9 show the observed FT-IR spectra of glucose (Figure 1b) and fructose (Figure 1c) particles produced by spraying 1.0 w/w % aqueous solutions, respectively. As was seen in the spectra of trehalose, rising baselines are observed in Figure 9a,b. In the Mie scattering calculations for glucose and fructose, we employed the refractive indices determined by Signorell et al.[10] As demonstrated in Figure 9, our experimental spectra were reproduced reasonably well by Mie calculations. The geometrical mean diameters defined in eq 3 were 110 and 100 nm for glucose and fructose, respectively, in agreement with the result for trehalose. On the other hand, the geometric standard deviation is smaller for glucose and fructose than for trehalose. This difference may be related to the viscosity of these solutions. The droplets of aqueous solutions of sugars undergo the glass transition, a transition from viscous liquid-like to vitreous solid-like behavior, during the evaporation process, in which the viscosity increases greatly. The aqueous solution of trehalose with the 50 mol % of glucose rings exhibits the glass transition at room temperature, while the other sugars undergo the transition at room temperature at the 80 and 100 mol % of glucose rings. Thus, the viscosity of the trehalose solution is expected to increase earlier than that of other sugars in the spray drying process.

Conclusion

Spray drying offers a simple method to generate amorphous nanoparticles, and that FT-IR spectroscopy combined with Mie analysis[20,27] can characterize these particles. Our results are in accord with a previous report on the formation of amorphous materials due to rapid solidification in the spray drying.[10] The difference, however, is that no heated gas was employed for solvent evaporation in this work. From the sizes of these solid particles, the droplet diameters prior to drying were estimated to be about 600 nm. Since the molecular solubility of amorphous nanoparticles is often at least an order of magnitude greater than that of crystalline nanoparticles,[29] as expressed by the Noyes−Whitney equation,[30] reduction of particle size is a promising way to improve the bioavailability of poorly soluble materials. Although this work focused on the production of nanoparticles by spraying aqueous solutions, the method is extendable to poorly water-soluble compounds in organic solvents or organic/aqueous cosolvents.[31]

References and Notes

(1) Lipinski, C. A.; Lombardo, F.; Dominy, B. W.; Feeney, P. J. *Adv. Drug Delivery Rev.* **1997**, *23*, 3–25.
(2) Lipinski, C. A. *Adv. Drug Delivery Rev.* **2001**, *46*, 3–26.
(3) Chen, R.; Tagawa, M.; Hoshi, N.; Ogura, T.; Okamoto, H.; Danjo, K. *Chem. Pharm. Bull.* **2004**, *52*, 1066–1070.
(4) Chen, R.; Okamoto, H.; Danjo, K. *Chem. Pharm. Bull.* **2006**, *54*, 948–953.
(5) Mizoe, T.; Beppu, S.; Ozeki, T.; Okada, H. *J. Controlled Release* **2007**, *120*, 205–210.
(6) Matsumura, Y.; Maeda, H. *Cancer Res.* **1986**, *46*, 6387–6392.
(7) Rasenack, N.; Müller, B. M. *Pharm. Dev. Technol.* **2004**, *9*, 1–13.
(8) Sen, D.; Spalla, O.; Taché, O.; Haltebourg, P.; Thill, A. *Langmuir* **2007**, *23*, 4296–4302.
(9) (a) York, P. *Pharm. Sci. Technol. Today* **1999**, *2*, 430–440. (b) Pasquali, I.; Bettini, R.; Giordano, F. *Eur. J. Pharm. Sci.* **2006**, *27*, 299–310.
(10) (a) Jetzki, M.; Signorell, R. *J. Chem. Phys.* **2002**, *117*, 8063–8073. (b) Signorell, R. *Chem. Phys. Lett.* **2000**, *329*, 52–60.
(11) Davis, B. G.; Robinson, M. A. *Curr. Opin. Drug Discovery Dev.* **2002**, *5*, 279–288.
(12) Rogers, J. C.; Kornfeld, S. *Biochem. Biophys. Res. Commun.* **1971**, *45*, 622–629.
(13) Elbein, A. D.; Pan, Y. T.; Pastuszak, I.; Carroll, D. *Glycobiology* **2003**, *13*, 17R–27R.
(14) Cesàro, A. *Nat. Mater.* **2006**, *5*, 593–594.
(15) Kilburn, D.; Townrow, S.; Meunier, V.; Richardson, R.; Alam, A.; Ubbink, J. *Nat. Mater.* **2006**, *5*, 632–635.
(16) Green, J. L.; Angell, C. A. *J. Phys. Chem.* **1989**, *93*, 2880–2882.
(17) Crowe, L. M.; Reid, D. S.; Crowe, J. H. *Biophys. J.* **1996**, *71*, 2087–2093.
(18) Chen, T.; Fowler, A.; Toner, M. L. *Cryobiology* **2000**, *40*, 277–288.
(19) Tanaka, M.; Machida, Y.; Niu, S.; Ikeda, T.; Jana, N. R.; Doi, H.; Kurosawa, M.; Nekooki, M.; Nukina, N. *Nat. Med.* **2004**, *10*, 148–154.
(20) Bohren, F. C.; Huffman, D. R. *Absorption and Scattering of Light by Small Particles*; Wiley: New York, 2004.
(21) Wolkers, W. F. A.; Oliver, E.; Tablin, F.; Crowe, J. H. *Carbohydr. Res.* **2004**, *339*, 1077–1085.
(22) Lucarini, V.; Saarinen, J. J.; Peiponen, K. E.; Vartiainen, E. M. *Kramers-Kronig Relations in Optical Materials Research*; Springer: Berlin, Germany, 2005.
(23) Ohta, K.; Ishida, H *Appl. Spectrosc.* **1988**, *42*, 952–957.
(24) Jeffrey, G. A.; Nanni, R. *Carbohydr. Res.* **1985**, *137*, 21–30.
(25) Foresman, J. B.; Frisch, Æ. In *Exploring Chemistry with Electronic Structure Methods*; Gaussian Inc.: Pittsburgh, PA, 1996.
(26) Imamura, K.; Maruyama, Y.; Tanaka, K.; Yokoyama, T.; Imanaka, H.; Nakanishi, K. *J. Pharm. Sci.* **2008**, *97*, 2789–2797.
(27) Mie, G. *Ann. Phys.* **1908**, *25*, 377–445.
(28) Sebhatu, T.; Angberg, M.; Ahlneck, C. *Int. J. Pharm.* **1994**, *104*, 135–144.
(29) Lindfors, L.; Forssén, S.; Skantze, P.; Skantze, U.; Zackrisson, A.; Olsson, U. *Langmuir* **2006**, *22*, 911–916.
(30) Noyes, A. A.; Whitney, W. R. *J. Am. Chem. Soc.* **1897**, *19*, 930–934.
(31) Hu, H. J.; Johnston, K. P.; Williams, R. O. *Eur. J. Pharm. Sci.* **2003**, *20*, 295–303.

JP9000835